

Mutations in the Central Domain of Potato Virus X TGBp2 Eliminate Granular Vesicles and Virus Cell-to-Cell Trafficking[▽]

Ho-Jong Ju, James E. Brown, Chang-Ming Ye, and Jeanmarie Verchot-Lubicz*

Department of Entomology and Plant Pathology, Oklahoma State University, Stillwater, Oklahoma 74078

Received 14 September 2006/Accepted 26 November 2006

Most RNA viruses remodel the endomembrane network to promote virus replication, maturation, or egress. Rearrangement of cellular membranes is a crucial component of viral pathogenesis. The PVX TGBp2 protein induces vesicles of the granular type to bud from the endoplasmic reticulum network. Green fluorescent protein (GFP) was fused to the PVX TGBp2 coding sequence and inserted into the viral genome and into pRTL2 plasmids to study protein subcellular targeting in the presence and absence of virus infection. Mutations were introduced into the central domain of TGBp2, which contains a stretch of conserved amino acids. Deletion of a 10-amino-acid segment (m2 mutation) overlapping the segment of conserved residues eliminated the granular vesicle and inhibited virus movement. GFP-TGBp2m2 proteins accumulated in enlarged vesicles. Substitution of individual conserved residues in the same region similarly inhibited virus movement and caused the mutant GFP-TGBp2 fusion proteins to accumulate in enlarged vesicles. These results identify a novel element in the PVX TGBp2 protein which determines vesicle morphology. In addition, the data indicate that vesicles of the granular type induced by TGBp2 are necessary for PVX plasmodesmata transport.

Most positive-strand RNA viruses cause specific changes in membrane architecture, creating distinct compartments for virus replication complexes. The types of membrane modifications include proliferations, invaginations, and novel vesicles or spherules. Proliferations are seen under the electron microscope as an expansion or increase in membrane layers. Invaginations, vesicles, or spherules often derive from the endoplasmic reticulum (ER), nuclear envelope, or organelles. These virus-induced compartments protect the replicating virus from host proteases and other defenses.

Poliovirus (PV), vaccinia virus, tobacco etch virus, cowpea mosaic virus, and brome mosaic virus are also examples of viruses which cause proliferation and invaginations of the ER for replication (8, 9, 12, 20, 41, 45, 48, 54). The membrane invaginations are containers for the viral replicase protecting the replication complexes from cellular degrading enzymes. Brome mosaic virus 1a is responsible for induction of vesicles, while the nature of the structures formed vary with the ratio of 1a:2a proteins (50, 51). When 2a is expressed at low levels, vesicles are induced. However, with increasing 2a concentrations, membranes accumulate in stacks rather than vesicles (51).

The tobacco mosaic virus (TMV) 126-kDa replicase protein induces membranous bodies to form in the absence of other TMV proteins. The TMV movement protein associates with these bodies and transports them along the microfilament network toward the periphery of the cell and, possibly, across the plasmodesmata (25, 30). Thus, TMV is the first plant virus that has been reported to involve membrane-bound replication complexes in the cell-to-cell transport pathway.

Beyond TMV, many plant viruses involve the endomem-

brane system in virus intracellular and intercellular movement. Examples of other viruses encoding small hydrophobic movement proteins which associate with the endomembrane system include the carmovirus (p9 and p8 proteins); panicovirus (ORF2 and ORF3 proteins; 6.6 and 14.6 kDa); closterovirus (p6 protein); potex-, carla-, allexi-, fovea-, hordei-, pomo-, and benyviruses (TGBp2 and TGBp3 proteins); and sobemovirus (p4 protein; 15 kDa) (16, 17, 22, 35–37, 42, 44, 55–57, 62, 63). Recent studies of potex- and pomoviruses report that endosomal or ER-related vesicles contribute to virus cell-to-cell movement (18, 23, 38).

Research in our laboratory focuses on the potexvirus potato virus X (PVX). PVX encodes three movement proteins from three overlapping open reading frames, termed the triple gene block (TGB). The TGB is conserved among viruses belonging to the genera *Potexvirus*, *Hordeivirus*, *Benyvirus*, *Carlavirus*, *Allexivirus*, *Foveavirus*, and *Pomovirus*. These three proteins are named TGBp1, TGBp2, and TGBp3 and are required for virus movement.

The PVX TGBp1 protein induces plasmodesma gating, moves from cell to cell, binds viral RNA, has ATPase activity, and forms inclusion bodies in virus-infected cells (4, 11, 13, 19, 32, 33, 46, 59). PVX TGBp1 is also a suppressor of RNA silencing, and a recent study showed this activity is necessary for virus cell-to-cell movement (6, 58). The PVX TGBp2 and TGBp3 proteins are ER-associated proteins (23, 28, 38, 49, 53, 62). PVX TGBp2 has two transmembrane segments and a central domain that is conserved among TGB-containing viruses (38). Amino acid sequence analyses of the potexvirus TGBp2 proteins identified two transmembrane segments and a central domain containing conserved amino acids (38) (see Fig. 1A). In the same study, two mutations, named m1 and m3 (see Fig. 1A), were introduced into the TGBp2 coding sequence and disrupted the transmembrane domains (38). These mutations inhibited virus cell-to-cell movement, indicating that membrane association of TGBp2 is necessary for virus move-

* Corresponding author. Mailing address: Oklahoma State University, 127 Noble Research Center, Stillwater, OK 74078. Phone: (405) 744-7895. Fax: (405) 744-6039. E-mail: verchot.lubicz@okstate.edu.

[▽] Published ahead of print on 6 December 2006.

ment (38). Electron microscopic analysis showed that the PVX TGBp2 protein induces formation of ER-derived vesicles during virus infection (23). While some have suggested these are transport vesicles carrying virus from the site of replication to the plasmodesmata, the role of these vesicles in virus movement has not been characterized (34).

TGBp3 has an N-terminal transmembrane segment and a variable C-terminal domain (28). Confocal and electron microscopic analysis showed that TGBp3 is in the ER. Colocalization experiments showed that the TGBp2 and TGBp3 proteins associate with the ER and peripheral bodies which may be ER-derived vesicles (18, 49, 53, 62, 63). A mutation disrupting the N-terminal transmembrane segment of TGBp3 eliminated ER association and inhibited virus cell-to-cell movement. Thus, membrane association of TGBp2 and TGBp3 is important.

In this study, we asked the following: are the granular vesicles induced by TGBp2 specifically needed for virus cell-to-cell movement, or is general remodeling of the ER network important? Here we identified a deletion mutation (m2) in the central domain of the TGBp2 protein which causes TGBp2 to accumulate in enlarged vesicles and in the ER network (see Fig. 1A). The same mutation inhibits virus movement. Further amino acid substitution mutations were used to characterize a segment of the PVX TGBp2 protein which modulates the vesicle phenotype. Single-amino-acid substitution mutations were enough to cause TGBp2 to associate with enlarged vesicles. These data indicate that specific granular vesicles induced by PVX TGBp2 drive virus cell-to-cell movement.

MATERIALS AND METHODS

Bacterial strains and plasmids. The *Escherichia coli* strains JM109, DH5 α , and XL10 Gold were used for transformation of all plasmids. J. Hasselof (Medical Research Council Laboratory of Molecular Biology, Cambridge, United Kingdom) (52) provided the pBIN-mGFP5-ER plasmid, used here to transform *Agrobacterium tumefaciens* strain LBA4404 to prepare transgenic BY-2 cultures.

The parental and mutant pPVX-GFP, pPVX-GFP:TGBp2, and pPVX-GFP:TGBp2m2 plasmids contain the PVX genome beside a bacteriophage T7 promoter (5). The plasmids pPVX-GFP and pPVX-GFP:TGBp2 contain the green fluorescent protein (GFP) or GFP-TGBp2 fused genes inserted next to the duplicated coat protein subgenomic promoter, as described previously (23). Nucleotide (nt) positions 5170 and 5423 were deleted within the viral genome in both the pPVX-GFP:TGBp2 and pPVX-GFP:TGBp2m2 plasmids (23). This mutation removes most of the TGBp2 coding sequence within the triple gene block (Fig. 1). The pPVX-GFP:TGBp2m2 plasmid (Fig. 1) is similar to pPVX-GFP:TGBp2 but has 30 nt deleted from the central domain of TGBp2 within the GFP-TGBp2 fused sequences (Fig. 1). The GFP-TGBp2m2 coding sequence was PCR amplified from pRTL2-GFP:TGBp2m2 plasmids using primers containing added ClaI and SalI restriction sites (38). The GFP-TGBp2m2 coding sequence was inserted into the PVX genomic cDNA between ClaI and SalI sites next to the duplicated coat protein subgenomic promoter (23).

The TGBp2 protein has a conserved amino acid sequence: G₅₂G₅₃XY₅₅XD₅₇G₅₈T₅₉K₆₀XI₆₂XY₆₄ (38). Substitution mutations were introduced into pPVX-GFP and pRTL2 plasmids using the Quick Change site-directed mutagenesis kit (Stratagene, La Jolla, CA). Three nucleotides encoding S (AGC) replaced Y₅₅ (TAC); nucleotides encoding A (GCC) or E (GAC) replaced D₅₇ (GAC); nucleotides encoding A (GCC) replaced T₅₉ (ACC); nucleotides encoding A (GCC) replaced K₆₀ (AAA); nucleotides encoding A (GCG) replaced I₆₂ (ATC); and nucleotides encoding S (AGC) replaced Y₆₄ (TAC). Mutagenic primers were extended using the prescribed temperature cycling regime. Sequences of the forward and reverse mutagenic primers are detailed in Table 1.

pRTL2-GFP, -GFP:TGBp2, -GFP:TGBp2m1, -GFP:TGBp2m2, and -GFP:TGBp2m3 were described previously (38). These plasmids contain the cauliflower mosaic virus (CaMV) 35S promoter and the tobacco etch virus translational enhancer (10) upstream of the coding sequences. The pRTL2-GFP:TGBp2 plasmid contains the GFP coding sequence fused to the 5' end of the

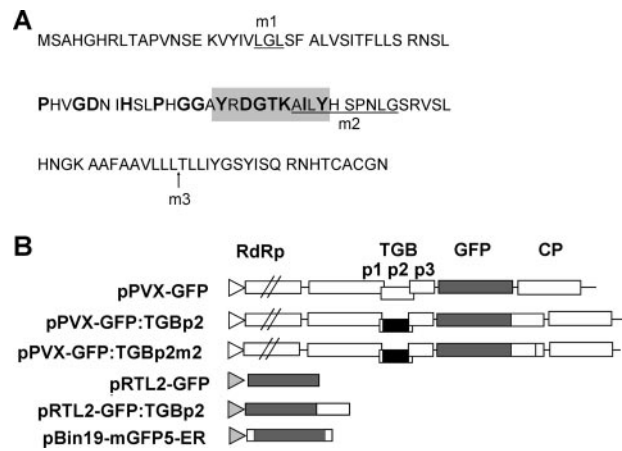


FIG. 1. Diagrammatic representation of plasmids used in this work. (A) The PVX TGBp2 amino acid sequence showing conserved residues (boldface) and variable residues (lightface). Ten substitution mutations replace six of the seven conserved residues highlighted in the gray box. The m1 mutation replaces a sequence encoding three amino acids, Leu-Gly-Leu (underlined), with a sequence encoding Ser-Arg-Pro. Ten amino acids (underlined) were deleted for the m2 mutation. The m3 mutation is an insertion mutation. A sequence encoding Ser-Arg-Pro was inserted at the position represented by the black arrow. (B) PVX infection clones and other plasmids used in this study. The name for each plasmid is indicated on the left. Open boxes represent PVX coding regions, and gray boxes represent the GFP coding sequence. The PVX genome consists of five open reading frames, named at the top of the panel. Abbreviations: RdRp, RNA-dependent RNA polymerase; TGB, triple gene block; CP, coat protein. The pPVX-GFP, pPVX-GFP:TGBp2, and pPVX-GFP:TGBp2m2 plasmids contain the bacteriophage T7 promoter (open triangle) and the PVX genomic cDNA. The pPVX-GFP plasmid contains the GFP coding sequence between the TGB and CP coding sequences. The pPVX-GFP:TGBp2 and pPVX-GFP:TGBp2m2 plasmids contain the GFP-TGBp2 and GFP-TGBp2m2 fusions in place of the GFP coding sequence. The black boxes represent deletion mutations in the TGBp2 coding sequences in the pPVX-GFP:TGBp2 and pPVX-GFP:TGBp2m2 plasmids. The pRTL2 constructs have a CaMV 35S promoter (gray triangle).

PVX TGBp2 coding sequence (29). pRTL2-GFP:TGBp2m1 contains a substitution mutation replacing 9 nt, TTAGGTCTA (encoding Leu-Gly-Leu), with AGTCGACCA (encoding Ser-Pro-Thr) from nucleotide positions 61 to 69 within the TGBp2 coding sequence (38). The pRTL2-GFP:TGBp2m2 plasmid has 30 nt deleted from the central domain of the TGBp2 coding sequence between nucleotide positions 181 and 210. pRTL2-GFP:TGBp2m3 has 9 nt, AGTCGACCA, inserted into the TGBp2 coding sequence following nucleotide position 263 within the TGBp2 coding sequence (38).

In vitro transcription. In vitro transcription was carried out using the pPVX-GFP, pPVX-GFP:TGBp2, and pPVX-GFP:TGBp2m2 plasmids and the mMACHINE High Yield capped RNA transcription kit (Ambion, Inc., Austin, TX). Plasmids were linearized using the SpeI enzyme. Transcripts were directly used to inoculate protoplasts or plants as described previously (23).

Inoculation of plants and RT-PCR analysis of mutant viruses. *Nicotiana benthamiana* plants were used for studying virus cell-to-cell and systemic movement (23). Five microliters of parental and mutant PVX-GFP, PVX-GFP:TGBp2, or PVX-GFP:TGBp2m2 transcripts was inoculated into an *N. benthamiana* plant dusted with carborundum. A handheld UV lamp was used to monitor virus cell-to-cell and vascular movement. In some plants, mutant viruses spread systemically. Total RNA was isolated from upper leaves of systemically infected plants using Triazol reagent (Invitrogen, Carlsbad, CA) (3). Reverse transcriptase (RT)-PCR was conducted using the Superscript III One-Step PCR system with Platinum *Taq* (Invitrogen) to amplify the entire TGB coding sequence. The TGB cDNAs were ligated to pGEM-T Easy plasmids (Promega Corp., Madison, WI) and used to transform JM109 cells. Three colonies were selected, and DNA

TABLE 1. Oligonucleotides used for mutagenesis of pRTL2-GFP:TGBp2 plasmids

Mutation ^a	Sequence of oligonucleotide ^b	
	Forward primer (5' to 3')	Reverse primer (5' to 3')
Y55S	CACGAGGAGCT AG CAGAGACGGCACC	GGTCCGCTCTGCTAGCTCCTCCGTG
D57A	GGAGGAGCTTACAGAG CC GGCACCAAAGCAATC	GATTGCTTTGGTGGCGGCTCTGATTGCTCCTCC
D57E	GGAGGAGCTTACAGAG AA GGCACCAAAGCAATC	GATTGCTTTGGTGGCT TCT CTGATTGCTCCTCC
T59S	GCTTACAGAGACGG CTCG AAAGCAATCTTG	CAAGATTGCTTT CG AGCCGCTCTGTGAAGC
T59A	GCTTACAGAGACGG CC CAAAGCAATCTTG	CAAGATTGCTTT GG CGCGCTCTGTGAAGC
K60A	GCTTACAGAGACGGCAC CC GGCAATCTTGAC	GTAGAAGATTG CG CGGTGCCGTCTGTGAAGC
K60R	GCTTACAGAGACGGCAC CC GGCAATCTTGAC	GTAGAAGATTG CG CGGTGCCGTCTGTAGC
I62A	GGCACCAAAG CAG CGTTGTACA ACT CCCC	GGGGAGTTGTACA AC GCTGCTTTGGTGCC
Y64S	CCAAAGCAATCTTG AG CAACTCCCCAAATC	GATTTGGGGAGTT GT CTCAAGATTGCTTTGG
Y64A	CCAAAGCAATCTTG GC CAACTCCCCAAATC	GATTTGGGGAGTT GG CCAAGATTGCTTTGG
m1	GTAAG T CGACCATCATTTGCTTTAGTTTCAATTACC	GATGG T CGACTTACTATGTACACTTTTTCAGAATTG
m2	GAGACGGCACCAA AT CACGAGTGAGTCTACACAA CGGAAAG	TTTGGTCCGCTCTCGTAAGCTCCTCC
m3	TGAG T CGCAACTTTGCTGATCTATGG	AAAG T TGGT CG ACTCAGTAGCAAAAACGGCAGCAAATGC

^a Each mutation was separately introduced into plasmid pRTL2-GFP:TGBp2. All plasmids except for the TGBp2m2 or TGBp2m3 plasmid introduce substitution mutations. The m2 mutation is a deletion mutation, and m3 is an insertion mutation.

^b Sequence of mutation is shown in boldface.

was isolated and sequenced. Sequencing results for all three colonies were identical for each mutant.

Preparation of transgenic BY-2 cells expressing mGFP5-ER. Transgenic BY-2 suspension cells expressing mGFP5-ER were used as a positive control for experiments studying the relationship of the PVX TGBp2 protein with the ER. Tobacco BY-2 suspension cells were transformed using *Agrobacterium tumefaciens* strain LBA4404 containing pBIN19-mGFP5-ER plasmids as described previously (21). Five milliliters of 3-day-old BY-2 suspension cells and 100 μ l of *Agrobacterium* suspension were mixed and coinoculated on petri plates containing BY-2 culture medium (4.3 g/liter Murashige and Skoog salts [Sigma, St. Louis, MO], 30 g/liter sucrose, 256 mg/liter KH_2PO_4 , 100 mg/liter myo-inositol, 1 mg/liter thiamine, and 0.2 mg/liter 2,4-dichlorophenoxyacetic acid, pH 5.6) plus 0.8% agar, for 2 days at 28°C in the dark. The tobacco BY-2 suspension cells were washed twice with 20 ml of BY-2 culture medium and then plated onto BY-2 selection medium (BY-2 culture medium plus 0.8% agar, 500 μ g/ml carbenicillin, and 300 μ g/ml kanamycin) and then maintained for 10 days at 28°C in the dark. The transgenic tobacco BY-2 suspension cells were then transferred to fresh BY-2 selection medium three times weekly. BY-2 suspension cells were examined with Olympus SZH-ILLK stereomicroscopy (Olympus Optical Co., Ltd., Japan) equipped with an excitation mercury lamp and GFP emission filter. Stably transformed BY-2 suspension cells were transferred to 250-ml Erlenmeyer flasks containing 50 ml of liquid BY-2 selection medium (BY-2 culture medium plus 200 μ g/ml kanamycin).

Nontransgenic and transgenic BY-2 suspension cells (39) were maintained on a rotary shaker at 120 rpm in a growth chamber at 28°C in the dark. Cultures were transferred each week into 250-ml Erlenmeyer flasks containing 50 ml of either fresh BY-2 culture medium or liquid BY-2 selection medium.

BY-2 protoplast preparation and transfection. Protoplasts were prepared from 3-day-old BY-2 suspension cells as described previously (15, 23, 43). To transfect protoplasts with infectious transcripts, 2 μ l (roughly 30 μ g) transcripts and 5×10^5 protoplasts (in 0.5 ml of solution 2) were mixed and transferred to a 0.4-cm-gap cuvette (Bio-Rad Laboratories, Hercules, CA) on ice. To transfect protoplasts with plasmids, 5 μ g plasmids, 40 μ g sonicated salmon sperm DNA, and 1×10^6 protoplasts (in 0.5 ml solution 2) were mixed and transferred to a 0.4-cm-gap cuvette on ice. Protoplasts were electroporated using a Gene Pulser (Bio-Rad Laboratories, Hercules, CA) at 0.25 kV, 100 Ω , and 125 μ F (23).

After electroporation, protoplasts were immediately transferred into a new tube containing 1 ml solution 2 and incubated on ice for 30 min and then at room temperature for 5 min. Protoplasts were collected by centrifugation at $79 \times g$ for 5 min, resuspended in 1.5 ml of BY-2 culture medium plus 0.45 M mannitol, and transferred to six-well cell culture plates (Corning, Corning, NY). The bottom of each well in the culture plates was coated with a solution of BY-2 culture medium plus 0.45 M mannitol and 1.0% agarose (pH 5.7). Transfected protoplasts were cultured at 26°C, collected at various times between 18 and 48 h by centrifugation at $79 \times g$ for 5 min, and then examined using laser scanning confocal microscopy (23).

Fluorometric assays and cycloheximide treatment of BY-2 protoplasts. A VICTOR2D fluorometer (Perkin-Elmer, Boston, MA) was used to measure

GFP expression in protoplasts transfected with the pRTL2-GFP, -GFP:TGBp2, or -GFP:TGBp2m2 plasmid (23). Samples of 1×10^6 protoplasts were harvested at 18, 24, 30, 36, and 48 h posttransfection and then transferred to liquid nitrogen. To measure protein turnover, the culture medium was removed from transfected protoplasts at 24 h posttransfection and replaced with fresh culture containing 500 μ M cycloheximide (Sigma, St. Louis, MO). Samples of 1×10^6 protoplasts were harvested at 0, 4, 8, and 12 h following addition of the cycloheximide (23) and transferred to liquid nitrogen.

One hundred microliters of protein grinding buffer (10 mM Tris-HCl, pH 7.5, 100 mM NaCl, 1 mM MgCl_2 , and 10 mM dichlorodiphenyltrichloroethane) was added to each sample. Samples were vortexed for 1 min, sonicated for 10 min, frozen at -80°C for 10 min, and then thawed at room temperature. Sample vortexing, sonication, freezing, and thawing were repeated. Following centrifugation at $3,000 \times g$ for 10 min, the supernatants of untreated and cycloheximide-treated extracts were used for fluorometric analyses. The average values from three samples at each time point were plotted using Microsoft Office Excel 2003 software (Microsoft Corp., Redmond, WA) (23).

Transient assays with tobacco leaves. *N. benthamiana* leaves were bombarded with pRTL2-GFP:TGBp2 and -GFP:TGBp2m2 transcripts using the PDS1000 He system (Bio-Rad) as described previously (30). Leaf segments were treated with FM4-64 dye and analyzed using confocal microscopy (19, 30).

Microscopy. A Leica TCS SP2 (Leica Microsystems, Bannockburn, IL) confocal laser scanning microscope was used to examine GFP, 4',6'-diamidino-2-phenylindole, and FM4-64 fluorescence (Molecular Probes Inc., Eugene, OR). The Leica TCS SP2 imaging system is attached to a Leica DMRE upright microscope with UV and Ar/Kr lasers. Images were compiled into figures using Adobe Photoshop CS software (Adobe Systems, Inc., San Jose, CA) (28, 29).

Statistical analysis. The SAS PROC CORR procedure using SAS 9.1 version (SAS Institute, Cary, NC) was used to test correlations between the percentages of protoplasts showing fluorescence in granular vesicles, the ER network, and enlarged vesicles (see Fig. 5). Tests compared granular vesicles and the ER network, enlarged vesicles and the ER network, or granular and enlarged vesicles for all mutant pRTL2-GFP:TGBp2 plasmids.

RESULTS

A deletion mutation in the central domain of TGBp2 inhibits virus cell-to-cell movement. The PVX-GFP:TGBp2 infectious clone was used to study the subcellular accumulation of TGBp2 during virus infection (23, 38). The GFP gene was fused to the 5' end of the TGBp2 coding sequences and inserted into the PVX infectious clone next to the duplicated coat protein subgenomic promoter. Most of the endogenous TGBp2 coding sequence was deleted from the PVX genome, and the GFP-TGBp2 fusion was a functional replacement. The

TABLE 2. Tobacco plants that are systemically infected with modified PVX viruses

Virus	Proportion of plants with systemic virus infection ^a
PVX-GFP.....	15/15
PVX-GFP:TGBp2.....	15/15
PVX-GFP:TGBp2m2.....	0/15
PVX-GFP-Y55S.....	0/12
PVX-GFP-D57A.....	0/12
PVX-GFP-D57E.....	0/12
PVX-GFP-T59A.....	0/12
PVX-GFP-K60A.....	0/12
PVX-GFP-I62A.....	1/12 ^b
PVX-GFP-Y64S.....	5/27 ^b

^a Proportions represent numbers of *N. benthamiana* plants showing fluorescence in upper noninoculated leaves by 16 dpi relative to the total number of plants inoculated with each virus.

^b RNA was isolated from systemically infected plants, RT-PCR was conducted, and PCR products were sequenced. Sequencing results show mutations reverted to wild-type sequence.

PVX-GFP infectious clone expresses GFP alone and was used as a control (Fig. 1B) (23, 38). For both PVX-GFP:TGBp2 and PVX-GFP, fluorescence was detected in inoculated tobacco leaves as early as 3 days postinoculation (dpi) and in upper leaves by 6 dpi (Table 2).

Infection foci on the inoculated leaves were studied using confocal microscopy to assess changes in subcellular distribution of the fusion protein over time. Each infection focus contains cells representing early and late infection events. The leading edge of infection contains newly infected cells and should provide insight into where proteins accumulate prior to or during virus transport across plasmodesmata. Cells located at the center of infection represent late stages of infection and should provide insight into where proteins accumulate after virus has moved into adjacent cells.

In PVX-GFP-inoculated leaves, fluorescence occurred in the cytoplasm and nucleus in all infected cells (Fig. 2A and B). Perinuclear inclusion bodies were also observed in PVX-GFP-infected cells (Fig. 2B and C). These are likely X-bodies, described in the early literature as masses containing virus particles, ER, and ribosomes (2, 26, 27). In previous reports describing the formation of X-bodies, they were often referred to as centers for virus replication, translation, and encapsidation (2, 14, 26, 27). The pattern of fluorescence seen in PVX-GFP-infected cells was similar at the center and leading edge of infection.

In cells located at the center of PVX-GFP:TGBp2 infection foci, we observed fluorescence in perinuclear inclusion bodies, in the ER network, and in granules (Fig. 2D, E, and F). In cells located at the center of infection, we see a clear ER network, granular vesicles, and perinuclear X-bodies (Fig. 2E). In cells located at the leading edge of infection, GFP-TGBp2 fluorescence was mainly in perinuclear bodies and granular vesicles (Fig. 2F). Fluorescence was faint in the ER network. A previous study explored fluorescence accumulation in PVX-GFP:TGBp2-infected tobacco protoplasts and found fluorescence in granular vesicles as early as 12 h postinoculation (23). These combined studies suggest that the TGBp2-related granular vesicles appear early in virus infection.

In a related study, we compared the accumulation of GFP-

TGBp2 and GFP-TGBp3 in plasmid-transfected and transgenic tobacco leaves using confocal and electron microscopy (23). GFP-TGBp2 and GFP-TGBp3 were both reported in the ER; however, the granular vesicles were seen only in GFP-TGBp2-expressing samples (23). These granular vesicles contained ribosomes, and immunolabeling detected BiP (an ER resident protein) in these vesicles (23). We also reported that these granular vesicles accumulate in tobacco leaves infected with PVX-GFP:TGBp2. Thus, the granules reported in Fig. 2E and F are the same granular vesicles induced by TGBp2 that were described in a previous study (23).

The m2 mutation is a deletion mutation that eliminates 10 amino acids in the central domain of the TGBp2 protein (Fig. 1A) (38). This mutation overlaps a segment of highly conserved amino acids. While previous experiments showed that the m2 mutation had no effect on ER association of the TGBp2 protein (38), its impact on vesicle formation was unexamined. We introduced the m2 mutation into the PVX-GFP:TGBp2 infectious clone to study the mutation's effects on virus cell-to-cell movement. Plants inoculated with PVX-GFP:TGBp2m2 were monitored for 3 weeks, and fluorescence was restricted to single cells (Fig. 2E; also Table 2). Fluorescence in these single cells was mainly in the ER network and in bright fluorescent bodies (Fig. 2F, G, and H). The small granular vesicles were rare. When we analyzed the bright fluorescent bodies at highest magnification, we discovered they were comprised of enlarged vesicles (Fig. 2H). The X-bodies seen in PVX-GFP- or PVX-GFP:TGBp2-infected cells were also "bright fluorescent bodies." However, at the highest resolution these resembled amorphous masses. We never observe enlarged vesicles in the X-bodies. Thus, these data suggest that the enlarged vesicles seen in plants inoculated with PVX-GFP:TGBp2m2 transcripts result from the m2 mutation.

The diameters of 50 granular and 50 enlarged vesicles were measured. The average diameter of the granular vesicles was $0.5 \mu\text{m} \pm 0.1 \mu\text{m}$, and that of the enlarged vesicles was $1.4 \mu\text{m} \pm 0.5 \mu\text{m}$. The dimensions of the granular vesicles measured in this study were similar to the dimensions measured previously using electron micrographs (23).

Subcellular localization of fluorescent proteins during virus infection in protoplasts. To view early events in virus infection, protoplasts were transfected with PVX-GFP, PVX-GFP:TGBp2, or PVX-GFP:TGBp2m2 transcripts and then analyzed at 18, 24, 36, and 48 h postinoculation (hpi) using confocal microscopy. Protoplasts expressing mGFP5-ER were included for comparison (Fig. 3A).

Between 18 and 48 hpi, fluorescence was visible in the cytoplasm and nuclei of PVX-GFP-infected protoplasts, as expected (Fig. 3B). In PVX-GFP:TGBp2-infected protoplasts, fluorescence was mainly in granular vesicles (Fig. 3C) (23). At all time points, PVX-GFP:TGBp2m2-infected protoplasts showed fluorescence mainly in the ER and enlarged vesicles (Fig. 3D, F, and H). There were fewer granular vesicles (Fig. 3D). A strand of ER surrounds the nucleus and can be seen in most protoplasts. At higher magnification, some of the enlarged vesicles appeared to be associated with strands of perinuclear or cortical ER (Fig. 3D, G, and I).

Subcellular targeting of wild-type and mutant GFP-TGBp2 proteins in leaves. Tobacco leaves were bombarded with pRTL2-GFP:TGBp2 or pRTL2-GFP:TGBp2m2 plasmids and

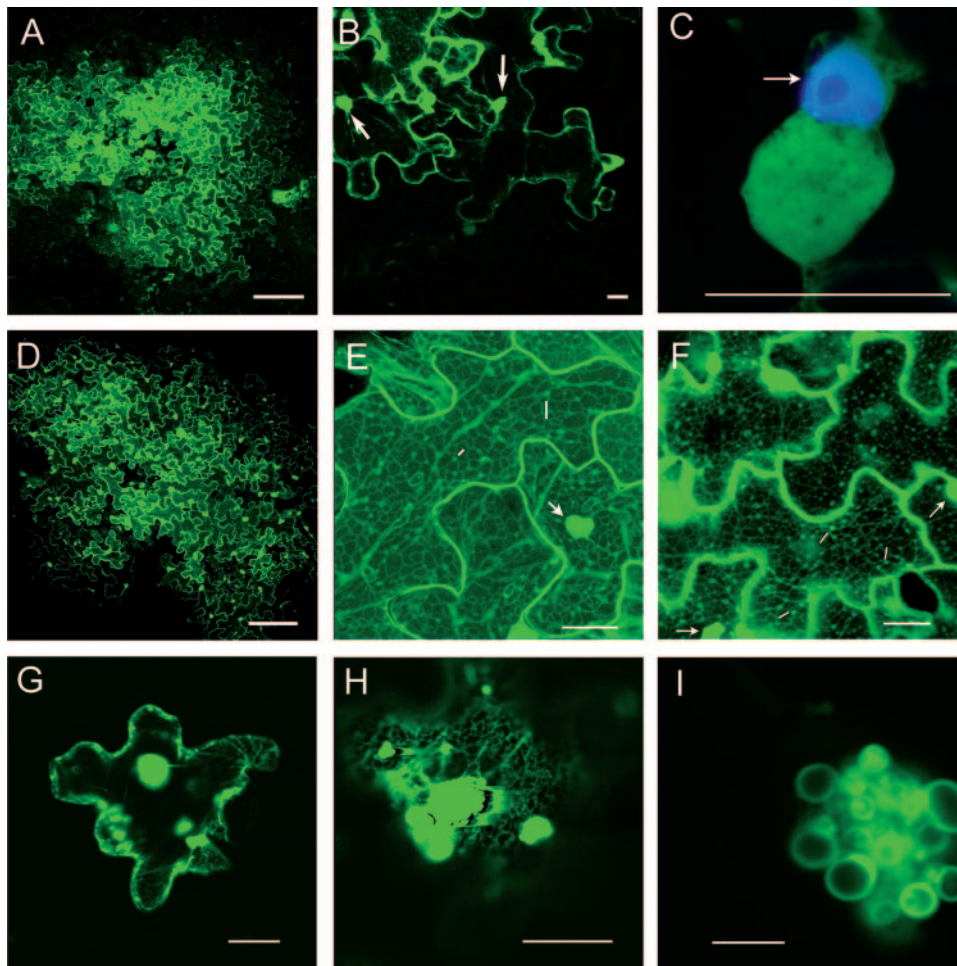


FIG. 2. Confocal images of PVX-infected tobacco leaves. (A) Image of infection focus on a PVX-GFP-inoculated leaf taken at roughly 4 dpi. Image was taken in a single optical plane. (B) Image taken at 4 dpi of epidermal cells at the leading edge of PVX-GFP infection. Resulting image is a maximum projection of nine serial sections taken at 2.5- μm intervals. Fluorescence is mainly cytosolic. Arrows point to nucleus. (C) At high magnification, X-bodies are seen neighboring the nucleus. Cells were treated with 4',6'-diamidino-2-phenylindole to differentiate the nucleus from the X-body. (D) Image taken at 4 dpi of infection focus on a PVX-GFP:TGBp2-infected leaf. Image taken in a single optical plane. (E) Image of epidermal cells located at the center of a PVX-GFP:TGBp2 infection focus. Image is a maximum projection of 12 optical sections taken in 1.3- μm steps. Image shows fluorescence in the ER network and in granular vesicles. Lines point to representative examples of granular vesicles; arrow points to nuclei and neighboring X-bodies. (F) Image of epidermal cells located at the leading edge of a PVX-GFP:TGBp2 infection focus. Image was taken in a single plane. Cells at the leading edge have mostly granular vesicles and X-bodies. Cells just behind the leading edge show faint ER network. (G, H, and I) Images of a single epidermal cell infected with PVX-GFP:TGBp2m2 taken at 6 dpi. Each image was taken in a single plane. (G) Image shows fluorescence in ER strands and large fluorescent bodies near the center and periphery of the cell. (H) Image taken at high magnification shows fluorescence in the ER. Bright fluorescent bodies are seen. (I) Highest magnification shows that fluorescent bodies contain enlarged vesicles. For this image, the Gain values were lowered to reduce brightness. This improves resolution of the enlarged fluorescent vesicles. When we reduced the Gain to resolve the structure of X-bodies in PVX-GFP- and PVX-GFP:TGBp2-infected cells, we saw an amorphous mass with no real form. We never found enlarged vesicles in X-bodies. Bars in panels A and D represent 200 μm . Bars in panels B, C, E, F, G, and H represent 20 μm . Bar in panel I represents 4 μm .

treated with FM4-64 dye. GFP-TGBp2 was seen in granular vesicles, and GFP-TGBp2m2 accumulated mainly in the ER and enlarged vesicles (Fig. 4A and D). Since previous studies indicated that the GFP-TGBp2-related vesicles were novel structures derived from the ER, we decided to conduct further tests to determine if the granular or enlarged vesicles are related to the plasma membrane or endocytic structures. Red fluorescence due to FM4-64 dye is initially seen in the plasma membrane and in endocytic vesicles budding from the plasma membrane. Following prolonged incubation, endocytic vesicles carry FM4-64 dye into the Golgi and vacuole. Thus, FM4-64 is

used to trace the endocytic pathway from the plasma membrane to the Golgi and vacuole (7). FM4-64 dye does not label the ER or nuclear envelope (7).

In Fig. 4, FM4-64 labeled the plasma membrane and endocytic vesicles. Leaf samples were incubated with FM4-64 dye between 30 min and 3 h, and we never detected red fluorescence in the TGBp2-related granular vesicles (Fig. 4A, B, and C). While the granular and endocytic vesicles often neighbored each other alongside the plasma membrane, the red and green signals never appeared to overlap. Similar observations were made with GFP-TGBp2m2. The GFP-TGBp2m2 enlarged ves-

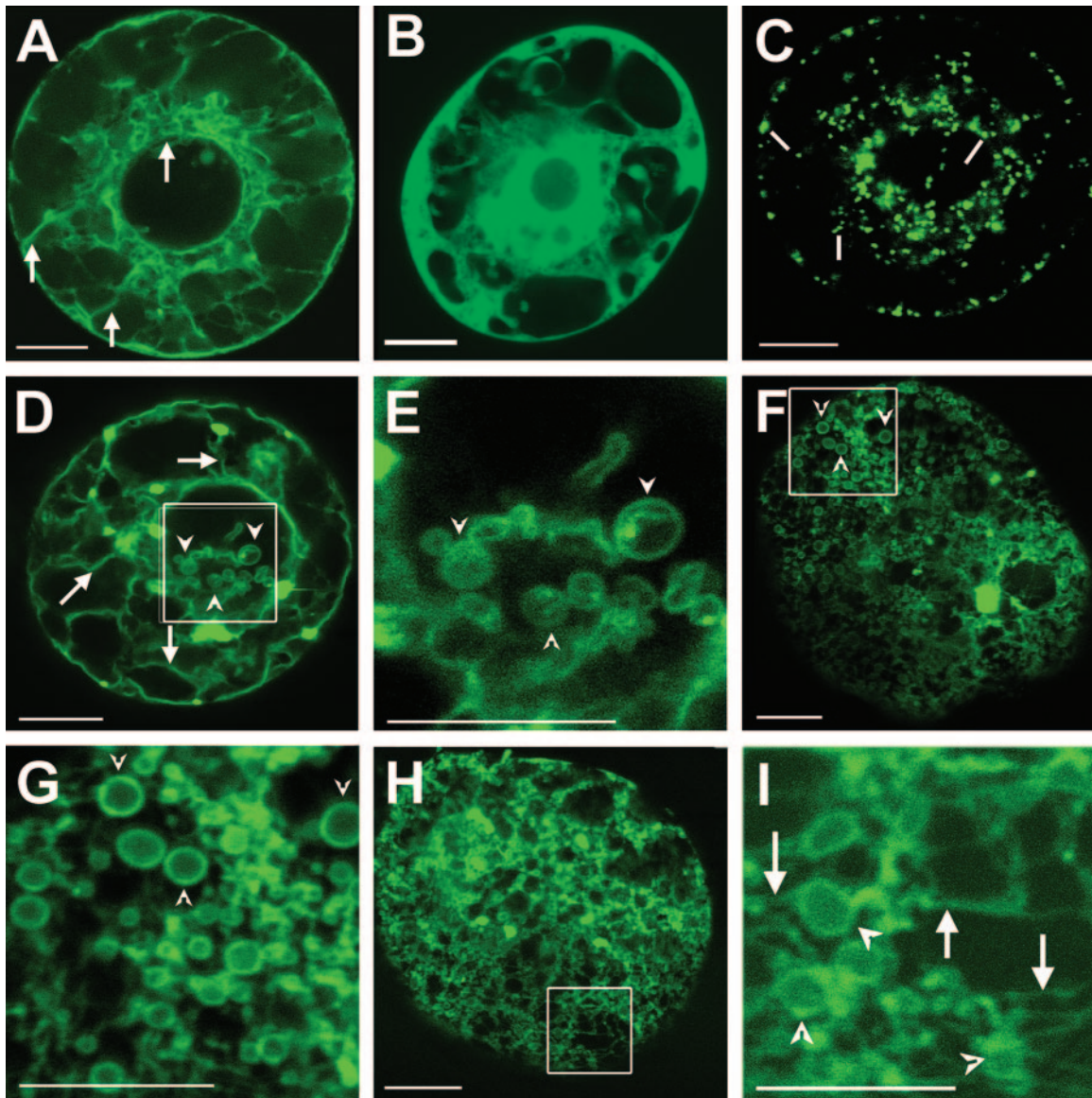


FIG. 3. Confocal images show fluorescence patterns in virus-infected protoplasts. In each panel, arrows point to perinuclear and cortical ER, straight lines point to representative examples of granular vesicles, and arrowheads point to enlarged vesicles. (A) Protoplasts expressing mGFP5-ER. (B) Protoplast inoculated with PVX-GFP shows fluorescence in the nucleus and cytoplasm. Image was taken at 24 hpi. (C) Image of protoplast inoculated with PVX-GFP:TGBp2 at 24 hpi. (D and E) Images of PVX-GFP:TGBp2m2-inoculated protoplast at 24 hpi. Box highlights enlarged vesicles, which appear to bud from the perinuclear ER. (E) View at high magnification of enlarged vesicles seen in the box in panel D. (F, G, H, and I) Images of PVX-GFP:TGBp2m2-inoculated protoplast at 48 hpi. Panels F and H show condensed ER network. Many enlarged vesicles occur throughout the cortical region of the protoplasts. (G and I) View at high magnification of enlarged vesicles seen in the box in panels F and H, respectively. At high magnification, the enlarged vesicles seem tethered by strands of ER. These images suggest the budding process might be disrupted by the m2 mutation. Bars in all panels represent 10 μ m.

icles were seen along the perinuclear ER and the plasma membrane (Fig. 4E and F). Endocytic vesicles seen budding from the plasma membrane often neighbored GFP-TGBp2m2-related vesicles. However, the red and green signals do not overlap (Fig. 4F and G). Thus, the GFP-TGBp2- and GFP-TGBp2m2-induced vesicles were unrelated to the plasma membrane or endocytic pathway.

Subcellular targeting of wild-type and mutant GFP-TGBp2 proteins in protoplasts. Five pRTL2 plasmids containing the GFP, GFP-TGBp2, GFP-TGBp2m1, GFP-TGBp2m2,

or GFP-TGBp2m3 coding sequence were transfected into BY-2 protoplasts. Prior investigations showed that the m1 and m3 mutations lie in the transmembrane domains, while the m2 mutation lies in the central conserved domain (Fig. 1A) (38). Since m1, m2, and m3 lie in separate subdomains of TGBp2, these experiments were designed to determine if the central conserved domain of TGBp2 is functionally distinct from the transmembrane domains. The subcellular accumulation patterns seen here in protoplasts were also confirmed with bombarded leaves (Fig. 4A) (23, 38).

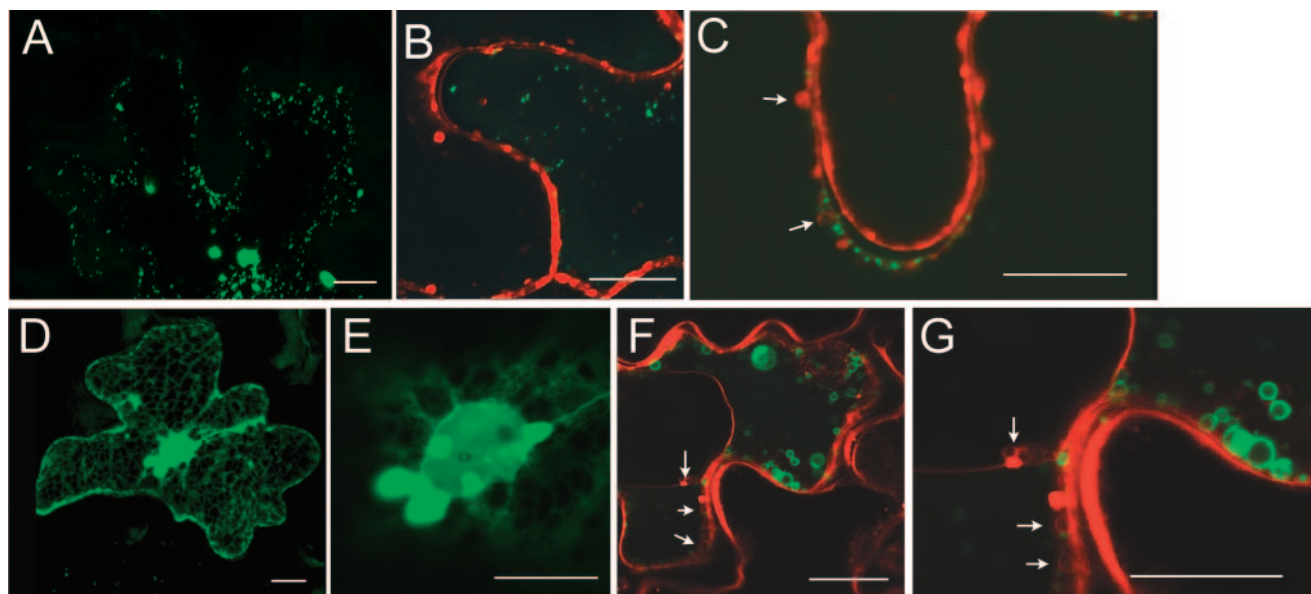


FIG. 4. Confocal images of tobacco leaf epidermal cells bombarded with pRTL2-GFP:TGBp2 or -GFP:TGBp2m2 and treated with FM4-64 dye. In each panel, arrows point to endocytic vesicles budding from the plasma membrane. (A, B, and C) Images show GFP-TGBp2 fluorescence in granular vesicles. FM4-64 stains the plasma membrane. (D, E, F, and G) Images show GFP-TGBp2m2 in the ER and enlarged vesicles. (E) Image shows vesicles budding from the perinuclear ER. (F and G) Images of an epidermal cell and the base of a trichome. FM4-64 stains both the epidermal cell and neighboring trichome. Green fluorescent vesicles neighbor endocytic vesicles along the plasma membrane. Bars represent 10 μ m.

GFP-TGBp2 fluorescence was mainly associated with granular vesicles at 24 h posttransfection (Fig. 5A). Sometimes we detected fluorescent aggregates in pRTL2-GFP:TGBp2-transfected protoplasts which were not detected in PVX-GFP-TGBp2-infected protoplasts. These aggregates may be aggregates of granular vesicles or artifacts resulting from protein overexpression from a CaMV 35S promoter. GFP-TGBp2m1 and GFP-TGBp2m3 fluorescence accumulated in the cytoplasm and nucleus (Fig. 5B and E). The m1 and m3 mutations, which lie in the transmembrane domains of TGBp2, disrupted ER association of GFP-TGBp2, as reported previously (38). GFP-TGBp2m2 fluorescence associated with enlarged vesicles and the perinuclear and cortical ER (Fig. 5C and D) (38). Granular vesicles were rare in GFP-TGBp2m2-expressing cells. This pattern of fluorescence resembled observations with PVX-GFP:TGBp2m2-inoculated plants and protoplasts. Thus, the m2 mutation, disrupting the central conserved domain of TGBp2, caused the protein to accumulate in the ER and in enlarged vesicles.

To determine if the enlarged vesicles were rare or common occurrences in GFP-TGBp2- and GFP-TGBp2m2-expressing cells, the presence of fluorescence in the ER network and granular and enlarged vesicles was quantified (Fig. 6A and B). For comparison, protoplasts expressing GFP only or mGFP5-ER were also quantified (Fig. 6B). Plasmids containing mGFP5-ER encode a version of GFP that has an N-terminal basic chitinase signal peptide and a C-terminal HDEL sequence for ER targeting and retention. One hundred percent protoplasts (30/30) expressing GFP contained fluorescence in the cytosol and nucleus (data not shown). GFP fluorescence was not membrane associated (Fig. 6B). This is contrasted by mGFP5-ER, where 100% (15/15) of protoplasts contained fluorescence in the ER network.

Granular and enlarged vesicles were absent from mGFP5-ER-expressing protoplasts (Fig. 6B).

Ninety-five percent of GFP-TGBp2-expressing protoplasts (19/20) contained fluorescence in granular vesicles, and 5% showed fluorescence in the ER (1/20) (Fig. 6A). As expected, 100% of GFP-TGBp2m1- and GFP-TGBp2m3-expressing protoplasts contained fluorescence in the cytosol and nucleus and not in the ER or vesicles (Fig. 6B). In GFP-TGBp2m2-expressing protoplasts, 86% contained fluorescence in the ER and 80% contained enlarged vesicles, while only 7% contained granular vesicles (Fig. 6A). Since a greater proportion of GFP-TGBp2m2-expressing protoplasts contained enlarged vesicles than contained granular vesicles, these data indicate that the m2 mutation caused GFP-TGBp2 to accumulate in enlarged vesicles.

Wild-type and mutant GFP-TGBp2 fusion proteins have similar half-lives. Clearly the m1, m2, and m3 mutations altered the subcellular distribution patterns of GFP-TGBp2 fluorescence. The best explanation is that these mutations disrupt targeting sequences in the PVX TGBp2 protein. However, it is also possible that the mutations alter the stability of TGBp2, causing the fusion proteins to be targeted to the cytosol for degradation. Fluorometric assays were used to quantify GFP expression over time as a measure of both protein accumulation and degradation in BY-2 protoplasts (23). Transfected protoplasts were chased at 24 h with cycloheximide to halt protein synthesis. Fluorometric values were measured at 0, 4, 8, and 12 h following cycloheximide treatment, and the protein half-lives were calculated. The fluorometric values were normalized to the measurement at 0 h (this value was set at 100%). The data were plotted, and linear regression was used to calculate protein half-lives. We predicted that if protein

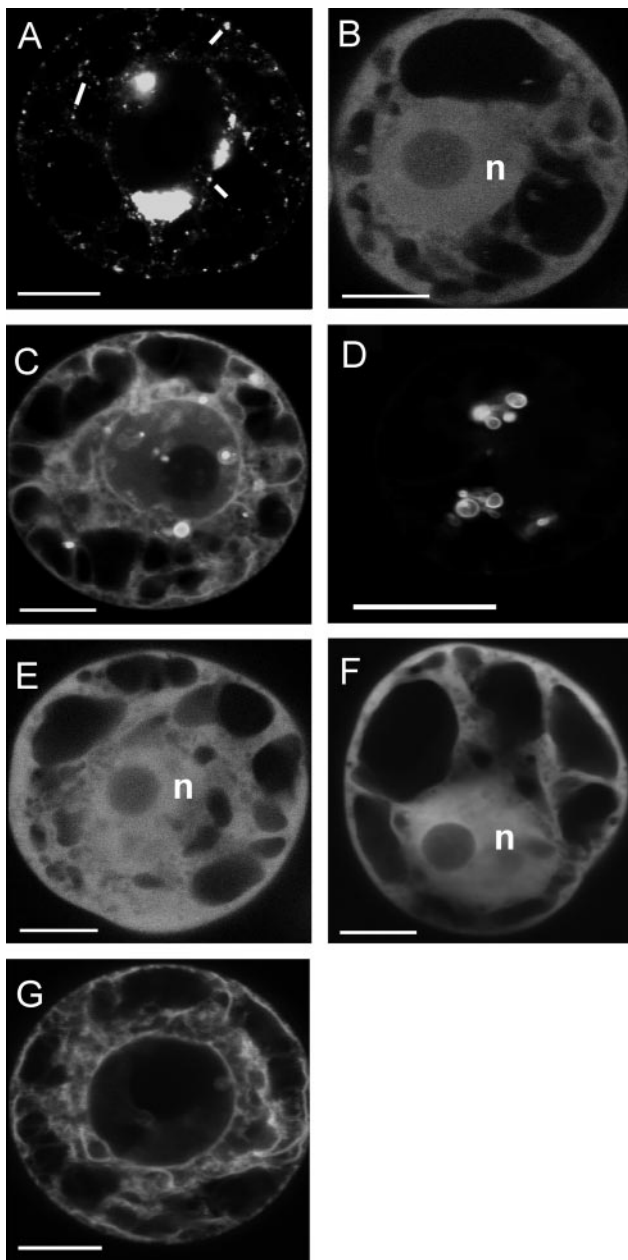


FIG. 5. Confocal images of protoplasts taken between 18 and 24 h posttransfection with pRTL2 plasmids. (A) Protoplast transfected with pRTL2-GFP:TGBp2, showing fluorescence in granular vesicles. Some vesicles aggregate in the perinuclear region. White lines point to a few representative granular vesicles. (B) Protoplast transfected with pRTL2-GFP:TGBp2m1, showing nuclear and cytosolic fluorescence. (C and D) Protoplasts transfected with pRTL2-GFP:TGBp2m2, showing ER network and enlarged vesicles. For this image, the Gain values were lowered to reduce brightness and improve resolution. With slightly higher Gain values, the ER network is seen (C), and resolution of the enlarged vesicles is reduced. (E) Protoplast transfected with pRTL2-GFP:TGBp2m3, showing nuclear and cytosolic fluorescence. (F) Protoplast transfected with pRTL2-GFP, showing nuclear and cytosolic fluorescence. (G) Transgenic protoplast expressing mGFP5-ER, showing fluorescence in the perinuclear and cortical ER. n, nucleus. Bars in all images except panel D represent 10 μ m. Bar in panel D represents 2 μ m.

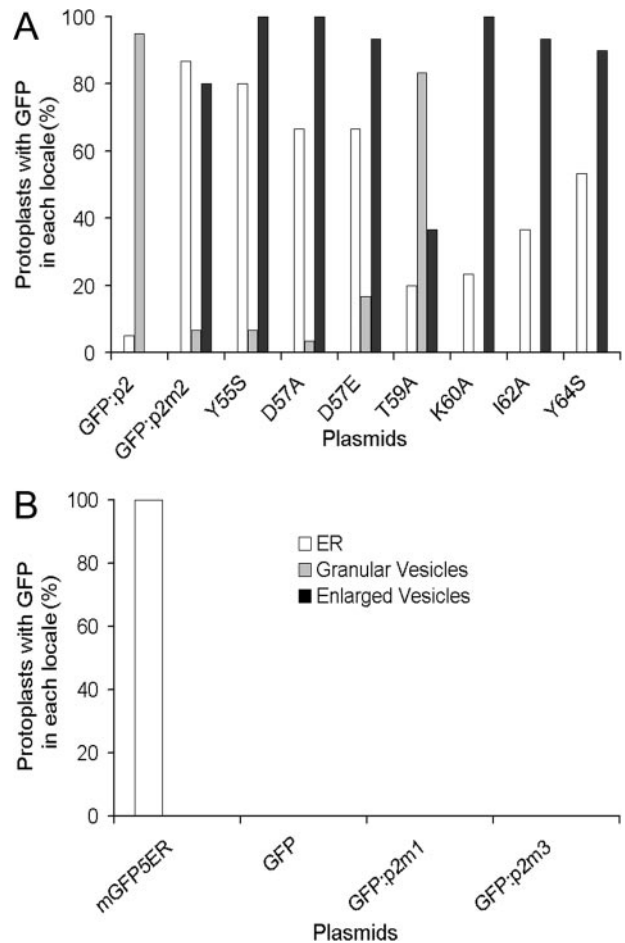


FIG. 6. Bar graphs depict the percentage of protoplasts containing fluorescence in the ER network, granular vesicles, and enlarged vesicles following transfection with pRTL2 plasmids. (A) Twenty protoplasts expressing GFP-TGBp2 and thirty protoplasts expressing each mutant GFP-TGBp2 protein were scored for fluorescence in each of the three subcellular domains. The percentages were compared statistically to determine a correlation between fluorescence in each subcellular domain. The statistics are provided in Results. (B) Control samples were scored for fluorescence in each of these domains but were not included in the statistical analysis. Fifteen mGFP5-ER-expressing and 30 GFP-, GFP-TGBp2m1-, and GFP-TGBp2m3-expressing protoplasts were scored.

turnover was stimulated as the result of the mutations, then fluorescence would decline more rapidly than in pRTL2-GFP- or -GFP:TGBp2-transfected protoplasts.

Fluorescence values measured in protoplasts transfected with pRTL2-GFP were higher than in protoplasts expressing the fusion proteins (Fig. 7A). Between 18 h and 48 h posttransfection, GFP values were three- to fivefold greater than GFP-TGBp2 values. In general, fluorometric values for all proteins seemed to fluctuate across a plateau between 24 and 48 h posttransfection (Fig. 7A) (23). Following addition of cycloheximide, the rate of decrease in GFP fluorescence was greater than the rate of decrease for wild-type and mutant GFP-TGBp2 fluorescence (Fig. 7B). Our calculation determined the half-life of GFP to be 10.2 h. The GFP-TGBp2, GFP-TGBp2m1, GFP-TGBp2m2, and GFP-TGBp2m3 pro-

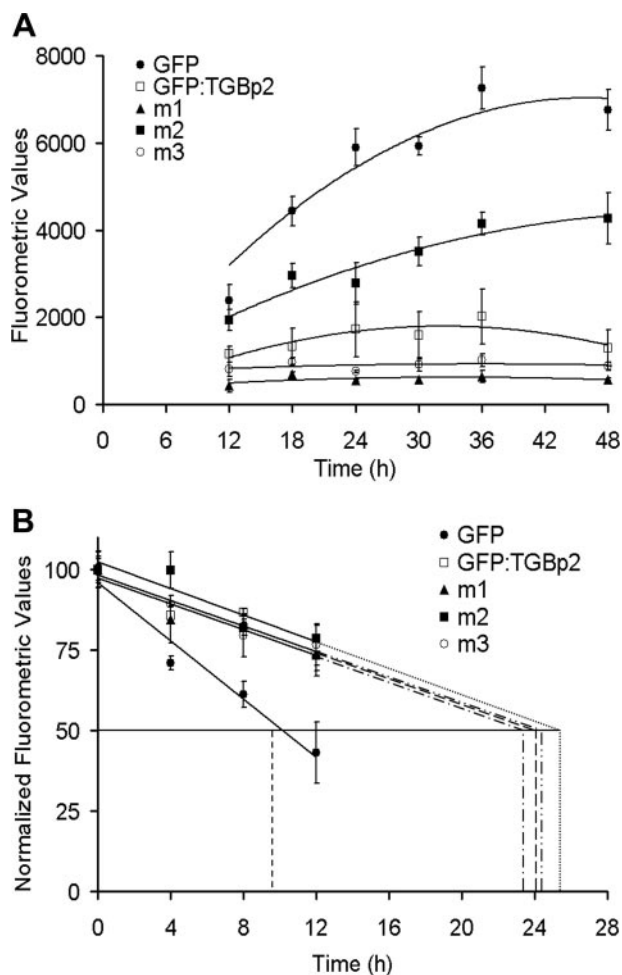


FIG. 7. Average fluorometric values in a time course analysis of BY-2 protoplasts transfected with pRTL2 plasmids. Each time point is the average of three fluorometric values. (A) Graph of the average fluorometric values for transfected protoplasts between 18 and 48 h posttransfection. A best-fit curve was determined using a second-order polynomial regression. (B) Transfected protoplasts were treated with cycloheximide at 24 h posttransfection. The average fluorometric values were normalized to time zero (24 h posttransfection) and then plotted using a linear regression. The horizontal line at 50 determines the half-life. The dotted lines represent the calculated protein half-lives determined by linear regression.

teins had similar half-lives of 24.5, 23.7, 25.5, and 24.3 h, respectively. The wild-type and mutant GFP-TGBp2 proteins were more stable than the nonfused GFP protein (Fig. 7B). Thus, changes in the subcellular distribution of mutant GFP-TGBp2 proteins were a specific result of the m1, m2, and m3 mutations rather than changes in protein stability.

Highly conserved amino acids regulate vesicle phenotype.

The m2 deletion mutation overlaps a highly conserved amino acid sequence in the TGBp2 protein (Fig. 1A). The highly conserved amino acids were identified in a prior study by aligning the amino acid sequences of TGBp2 proteins from nine potexviruses (38). If these conserved amino acid residues are essential to form granular vesicles, then single-substitution mutations might produce alternative membrane structures. Moreover, if enlarged vesicles were the result of a defect in the

ability of TGBp2 to form granular vesicles, then substitution of conserved amino acid residues would result in enlarged vesicles rather than granular vesicles.

Seven mutations encoding amino acid substitutions were introduced into pRTL2-GFP:TGBp2 plasmids, replacing Tyr55 with Ser; Asp57 with Ala or Glu; Thr59 with Ala; Lys60 with Ala; Ile62 with Ala; and Tyr64 with Ser. Protoplasts were transfected with mutant pRTL2-GFP:TGBp2 plasmids and viewed at 24 h posttransfection. A random set of 30 protoplasts was scored for the presence of fluorescence in the ER, granular vesicles, and enlarged vesicles.

Fluorescence occurred mainly in the ER and enlarged vesicles in protoplasts expressing GFP-TGBp2-Y55S, -D57A, -D57E, -K60A, -I62A, or -Y64S (Fig. 6A and 8). Between 0 and 17% of protoplasts contained a few granular vesicles. The reduction in granular vesicles due to these mutations resembles the reduction due to GFP:TGBp2m2. These data suggest that Tyr55, Asp57, Lys60, Ile62, and Tyr64 modulate the nature of vesicles associated with GFP-TGBp2 fluorescence (Fig. 6A and 8).

Replacing Thr59 with Ala increased the proportion of protoplasts containing enlarged vesicles, although granular vesicles were not eliminated (Fig. 6A and 8). The result of substituting Thr59 with Ala was not as significant as those with substitutions replacing Tyr55, Asp57, Ile62, and Tyr64 (Fig. 6A and 8), indicating that Thr59 is not as important as the other residues for determining the vesicle phenotype.

In comparing GFP-TGBp2 with each of the mutant proteins in Fig. 6A, it seems that deletion and substitution mutations which reduce protein accumulation in granular vesicles also increase accumulation in the ER and enlarged vesicles. Statistical analysis revealed an inverse correlation between granular and enlarged vesicles ($r = -0.96$; $P < 0.0001$) and between granular vesicles and the ER ($r = -0.66$; $P = 0.0551$). Fluorescence in enlarged vesicles and the ER network positively correlates ($r = 0.66$; $P = 0.0529$). Thus, a decline in granular vesicles is responsible for an increase in fluorescence in the ER and enlarged vesicles. Since TGBp2 induces vesicles from the ER network, the statistical data indicate that the mutations either cause TGBp2 to be redirected from granular into enlarged vesicles or alter vesicle morphology, causing enlarged vesicles to accumulate.

Substitution mutations inhibit PVX cell-to-cell movement.

Each substitution mutation was introduced into the PVX-GFP infectious clone to examine the effects of the single-amino-acid substitution mutations on virus cell-to-cell movement. Transcripts were prepared and inoculated into tobacco leaves to determine if the mutations had any effect on virus movement. GFP expression was used to monitor the spread of infection until 16 dpi. As mentioned previously, PVX-GFP infection was detected in inoculated leaves as early as 3 dpi and in upper leaves by 6 dpi. PVX-GFP-Y55S, -D57A, -D57E, -T59A, and -K60A were restricted to single cells in inoculated leaves (Table 2). These data indicate that mutations causing TGBp2 to accumulate in the ER and enlarged vesicles also inhibit virus cell-to-cell movement and that granular vesicles are important for virus cell-to-cell movement.

Between 8 and 18% of plants inoculated with PVX-GFP-I62A or -Y64S showed systemic virus accumulation. In these plants, GFP expression was detected in expanding infection

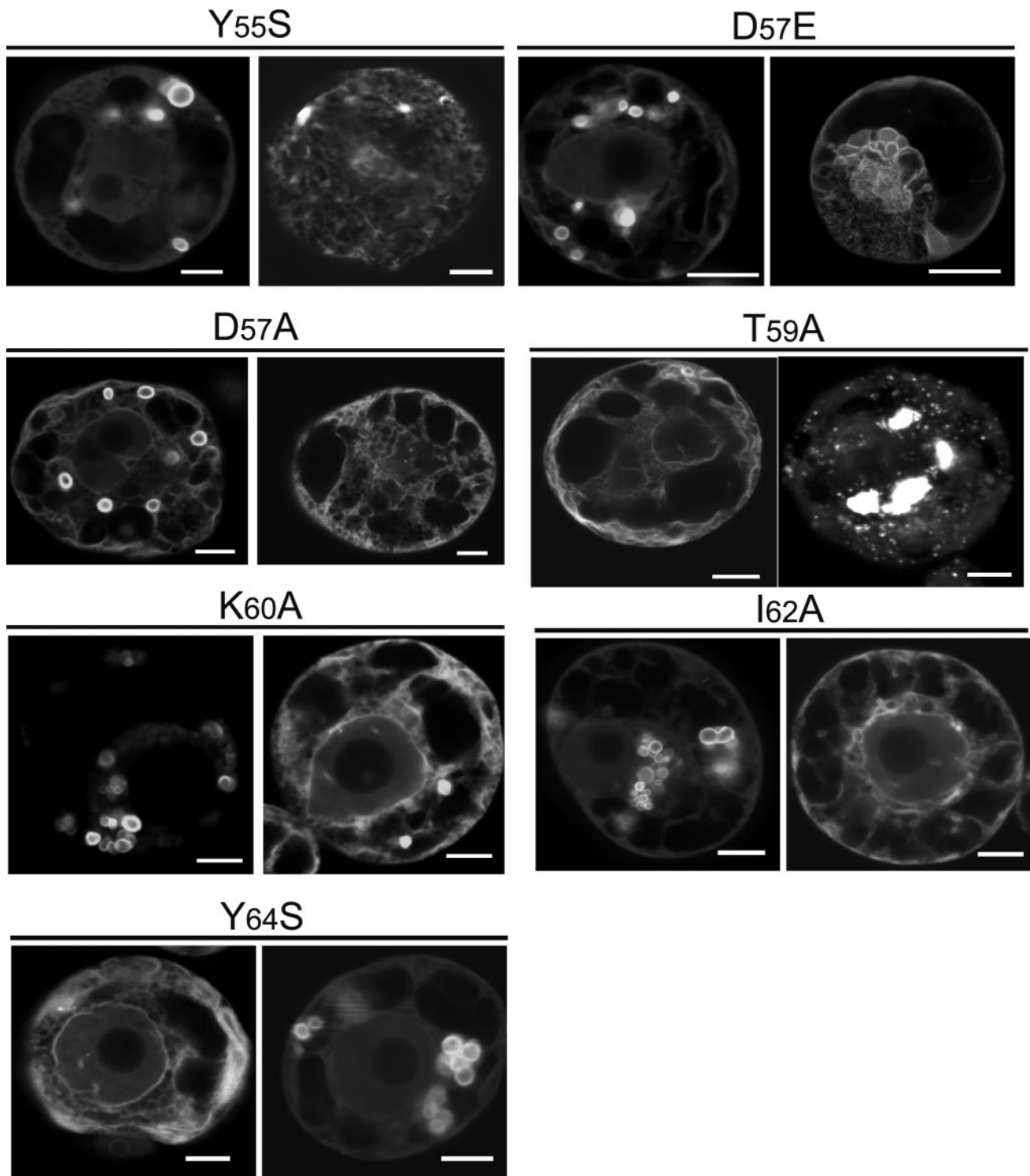


FIG. 8. Confocal images show protoplasts transfected with mutant pRTL2-GFP:TGBp2 plasmids at 24 h posttransfection. The panels are representative images for each substitution mutation. Each amino acid substitution mutation is identified above the corresponding panels. Bars in all images represent 10 μ m.

foci on the inoculated leaves by 7 dpi and on the upper leaves by 9 dpi. Virus movement was delayed relative to that of PVX-GFP. For all plants that showed systemic virus accumulation, RNA was isolated and RT-PCR was conducted to am-

plify the TGB coding region. PCR products were sequenced, and the systemically accumulating virus in plants inoculated with PVX-GFP-I62A or -Y64S did not contain the same mutation. Thus, virus movement was seen only when the muta-

tions reverted to the wild-type sequence. The same mutations causing GFP-TGBp2 to accumulate in enlarged vesicles also inhibited virus cell-to-cell movement (Table 2).

The T59A mutation caused GFP-TGBp2 to accumulate in enlarged vesicles and showed a high proportion of protoplasts containing granular vesicles. Since this mutation inhibited PVX cell-to-cell movement (Table 2), Thr59 likely contributes to other TGBp2 activities needed for virus movement, beyond regulating granular vesicle morphology.

DISCUSSION

In previous studies, we showed that GFP-TGBp2 accumulated in small granular vesicles when the fusion was expressed from the PVX genome in BY-2 protoplasts or infected leaves. We also saw the same granular vesicles when GFP-TGBp2 was expressed from the CaMV 35S promoter in BY-2 protoplasts, bombarded leaves, and transgenic tobacco leaves (23, 38). Using electron microscopy and cryoembedded samples, we presented evidence that these granular vesicles consist of ER membranes. These vesicles contain ribosomes, and immunolabeling detected BiP, an ER resident protein, in these vesicles (23) (data not shown). In this study, GFP-TGBp2-expressing cells were treated with FM4-64 dye, which is often used to trace membranes through the endocytic pathway. The red fluorescence observed in the plasma membrane and endocytic vesicles never overlapped with green fluorescence in the GFP-TGBp2-expressing vesicles. These data support previous evidence that the GFP-TGBp2-related vesicles are novel structures derived from the ER and are unrelated to the plasma membrane and endosome.

A study of potato mop top virus (PMTV) showed that TGB proteins associate with two types of vesicles: small granular vesicles and endocytic vesicles. The granular vesicles are described as transport vesicles carrying viral RNA to the plasmodesmata (18). In this model, these granular vesicles fuse with the plasma membrane (18). Prior studies showed that the PVX TGBp2-induced vesicles associate with the microfilament network (23). The PVX TGBp2-induced vesicles might traffic along microfilaments toward the plasmodesmata. For PMTV, evidence indicates that TGBp2 and TGBp3 proteins are recaptured from the plasma membrane by endocytic vesicles, which carry them back to the site of virus replication (18). While experiments using FM4-64 in this study did not detect PVX TGBp2 associating with the endosome, the results of mutational analysis indicate that the PVX TGBp2-induced granular vesicles are specifically required for virus cell-to-cell movement. Eight mutations were introduced into the central region of the PVX TGBp2 protein. One mutation deleted 10 amino acids, while 7 other mutations were substitutions replacing individual residues. Granular vesicles were absent from cells expressing the mutant GFP-TGBp2 proteins. Table 2 shows that these mutations also inhibited virus movement. These data suggest that PVX, similar to PMTV, requires these granular vesicles for virus movement.

TGBp2 has three domains: N-terminal and C-terminal transmembrane segments and a central sequence which lies in the ER lumen (61). The central domain of TGBp2 has a segment of highly conserved amino acid residues between positions 40 and 64. In this study, we introduced substitution

mutations replacing residues between position 55 and 64. These mutations increased GFP-TGBp2 association with the ER and enlarged vesicles while decreasing its association with granular vesicles. These data suggest that Tyr55, Asp57, Lys60, Iso62, and Tyr64 represent a segment of conserved amino acids which determine the nature of vesicles containing GFP-TGBp2 proteins.

One explanation for the enlarged vesicles is that the mutations had altered the subcellular targeting of GFP-TGBp2, causing the proteins to accumulate in the endosome rather than in the granular vesicles. To test this idea, cells expressing the mutant GFP-TGBp2 proteins were treated with FM4-64. The results indicate that the enlarged vesicles were not related to the endosome. Further evidence that the enlarged vesicles are not endocytic vesicles was presented in Fig. 3. In PVX-GFP:TGBp2-infected protoplasts, we observed enlarged vesicles associating with the nuclear envelope. In some instances we observed these vesicles tethered to the cortical ER network (Fig. 3I). The protoplast images in Fig. 3G and I suggest that the GFP-TGBp2m2 proteins may cause bubbles to form from the perinuclear and cortical ER which become enlarged vesicles. It is worth speculating that the enlarged vesicles result from defects in vesicle formation triggered by TGBp2. However, we cannot be certain whether the enlarged vesicles are the result of mutations that alter the dimensions of the vesicles, cause a defect in the budding process, or cause TGBp2 to be directed into another type of cellular vesicle. Further analysis is needed to characterize the identity or origin of these enlarged vesicles.

Since the central domain of TGBp2 lies in the interior of the ER, this sequence may interact with ER luminal factors, such as small GTPases (ARFs), which regulate vesicle formation. If TGBp2-induced vesicles function as transport vesicles, it is reasonable to consider that they may have features resembling plant transport vesicles. For example, formation of COPI, COPII, or post-Golgi vesicles typically involves ARFs, which are involved in the recruitment of coat proteins. These ARFs are crucial for vesicle budding and for fusion with target membranes (24, 40, 60). Perhaps TGBp2 associates with ARFs in the ER lumen to drive vesicle formation. Another possibility is that the central conserved domain of PVX TGBp2 is necessary for oligomerization of TGBp2 along the membrane surface. TGBp2 oligomers may cause deformation of ER membranes, leading to vesicle formation. Perhaps the mutations tested in this study functioned to weaken or inhibit TGBp2 oligomerization and thereby alter vesicle morphology. Further mutational analysis is needed to define the extent of the conserved sequence which may affect conversion of granular vesicles into enlarged vesicles and to determine if this sequence governs TGBp2 interactions with itself or cellular proteins.

Another explanation for the images in Fig. 3 showing enlarged vesicles tethered to the ER is that these vesicles are fusing with the ER. If the granular vesicles transport viral RNA to the cell surface, they could fuse with the cortical ER, releasing their contents into the plasmodesmata for transport into neighboring cells. In this scenario, the mutations may cause a defect in vesicles fusing with the ER, resulting in the enlarged bubbles that appear to be tethered to the ER network. This model requires granular vesicles are successfully produced, traffic to the periphery of the cell, associate with the

ER network near plasmodesmata, and get stuck while fusing with the ER. This could explain loss of movement for PVX-GFP-T59A. In protoplasts expressing GFP-TGBp2-T59A, we saw that 83% contained granular vesicles and 37% contained enlarged vesicles. This mutation had little effect on granular vesicles while causing an increase in enlarged vesicles. Loss of virus movement could occur if the mutation causes vesicles to get stuck and form bubbles while fusing to the ER and if vesicle fusion with the ER is important for virus movement. Further research is needed to define the origin and target of granular and enlarged vesicles.

Many RNA viruses cause ER modifications to promote virus replication or maturation (1, 8, 9, 12, 20, 41, 45, 47, 48, 54). These modifications influence protein sorting, secretion, membrane permeability affecting host defense responses, ER stress, and apoptosis (31). Real-time imaging of TMV has shown that the viral MP binds to membrane-bound replication complexes and carries these toward the plasmodesmata for cell-to-cell transport (25, 30). We do not yet know if PVX TGBp2 associates with the PVX replicase or, like TMV, moves replication complexes across the plasmodesmata. While evidence of membrane-bound bodies contributing to plasmodesmata transport has been described recently for TMV and PVX, this study is the first to use mutational analysis to show that virus-induced vesicles are necessary for intercellular trafficking.

ACKNOWLEDGMENTS

Support for this project was provided by National Science Foundation Integrative Plant Biology Program Award IBM-9982552 and in part by the Oklahoma Agriculture Experiment Station under project H-2371. Funding for research done by James Brown was supported by the LS-OKAMP and Native Americans in Biological Sciences (NABS) programs.

We thank J. Fletcher and S. Marek for use of their electroporation systems. We also thank Terry Colberg for training and assistance with the confocal microscope located at the Oklahoma State University Electron Microscopy Center.

REFERENCES

- Ahlquist, P., A. O. Noueiry, W. M. Lee, D. B. Kushner, and B. T. Dye. 2003. Host factors in positive-strand RNA virus genome replication. *J. Virol.* **77**:8181–8186.
- Allison, A., and T. Shalla. 1973. The ultrastructure of local lesions induced by *Potato virus X*: a sequence of cytological events in the course of infection. *Phytopathology* **64**:784–793.
- An, H., U. Melcher, P. Doss, M. Payton, A. C. Guenzi, and J. Verchot-Lubicz. 2003. Evidence that the 37 kDa protein of *Soil-borne wheat mosaic virus* is a virus movement protein. *J. Gen. Virol.* **84**:3153–3163.
- Angell, S. M., C. Davies, and D. C. Baulcombe. 1996. Cell-to-cell movement of *Potato virus X* is associated with a change in the size-exclusion limit of plasmodesmata in trichome cells of *Nicotiana clevelandii*. *Virology* **216**:197–201.
- Baulcombe, D. C., S. Chapman, and S. Santa Cruz. 1995. Jellyfish green fluorescent protein as a reporter for virus infections. *Plant J.* **7**:1045–1053.
- Bayne, E. H., D. V. Rakitina, S. Y. Morozov, and D. C. Baulcombe. 2005. Cell-to-cell movement of potato potexvirus X is dependent on suppression of RNA silencing. *Plant J.* **44**:471–482.
- Bolte, S., C. Talbot, Y. Boutte, O. Catrice, N. D. Read, and B. Satiat-Jeunemaitre. 2004. FM-dyes as experimental probes for dissecting vesicle trafficking in living plant cells. *J. Microsc.* **214**:159–173.
- Carette, J. E., M. Stuiver, J. Van Lent, J. Wellink, and A. Van Kammen. 2000. Cowpea mosaic virus infection induces a massive proliferation of endoplasmic reticulum but not Golgi membranes and is dependent on de novo membrane synthesis. *J. Virol.* **74**:6556–6563.
- Carette, J. E., J. van Lent, S. A. MacFarlane, J. Wellink, and A. van Kammen. 2002. Cowpea mosaic virus 32- and 60-kilodalton replication proteins target and change the morphology of endoplasmic reticulum membranes. *J. Virol.* **76**:6293–6301.
- Carrington, J. C., and D. D. Freed. 1990. Cap-independent enhancement of translation by a plant potyvirus 5' nontranslated region. *J. Virol.* **64**:1590–1597.
- Davies, C., G. Hills, and D. C. Baulcombe. 1993. Sub-cellular localization of the 25-kDa protein encoded in the triple gene block of *Potato virus X*. *Virology* **197**:166–175.
- den Boon, J. A., J. Chen, and P. Ahlquist. 2001. Identification of sequences in *Brome mosaic virus* replicase protein 1a that mediate association with endoplasmic reticulum membranes. *J. Virol.* **75**:12370–12381.
- Donald, R. G., D. M. Lawrence, and A. O. Jackson. 1997. The *Barley stripe mosaic virus* 58-kilodalton beta (b) protein is a multifunctional RNA binding protein. *J. Virol.* **71**:1538–1546.
- Espinoza, A. M., V. Medina, R. Hull, and P. G. Markham. 1991. *Cauliflower mosaic virus* gene II product forms distinct inclusion bodies in infected plant cells. *Virology* **185**:337–344.
- Gaire, F., C. Schmitt, C. Stussi-Garaud, L. Pinck, and C. Ritzenthaler. 1999. Protein 2A of grapevine fanleaf nepovirus is implicated in RNA2 replication and colocalizes to the replication site. *Virology* **264**:25–36.
- Gilmer, D., S. Bouzoubaa, A. Hehn, H. Guilley, K. Richards, and G. Jonard. 1992. Efficient cell-to-cell movement of *Beet necrotic yellow vein virus* requires 3' proximal genes located on RNA 2. *Virology* **189**:40–47.
- Grieco, F., M. A. Castellano, G. P. Di Sansebastiano, G. Maggipinto, J. M. Neuhaus, and G. P. Martelli. 1999. Subcellular localization and in vivo identification of the putative movement protein of *Olive latent virus 2*. *J. Gen. Virol.* **80**:1103–1109.
- Haupt, S., G. H. Cowan, A. Ziegler, A. G. Roberts, K. J. Oparka, and L. Torrance. 2005. Two plant-viral movement proteins traffic in the endocytic recycling pathway. *Plant Cell* **17**:164–181.
- Howard, A. R., M. L. Heppler, H.-J. Ju, K. Krishnamurthy, M. E. Payton, and J. Verchot-Lubicz. 2004. *Potato virus X* TGBp1 induces plasmodesmata gating and moves between cells in several host species whereas CP moves only in *N. benthamiana* leaves. *Virology* **328**:185–197.
- Husain, M., and B. Moss. 2003. Evidence against an essential role of COPII-mediated cargo transport to the endoplasmic reticulum-Golgi intermediate compartment in the formation of the primary membrane of vaccinia virus. *J. Virol.* **77**:11754–11766.
- Hwang, H. H., and S. B. Gelvin. 2004. Plant proteins that interact with VirB2, the *Agrobacterium tumefaciens* pilin protein, mediate plant transformation. *Plant Cell* **16**:3148–3167.
- Ivanov, K. I., P. A. Ivanov, E. K. Timofeeva, Y. L. Dorokhov, and J. G. Atabekov. 1994. The immobilized movement proteins of two tobamoviruses form stable ribonucleoprotein complexes with full-length viral genomic RNA. *FEBS Lett.* **346**:217–220.
- Ju, H. J., T. D. Samuels, Y. S. Wang, E. Blancaflor, M. Payton, R. Mitra, K. Krishnamurthy, R. S. Nelson, and J. Verchot-Lubicz. 2005. The *Potato virus X* TGBp2 movement protein associates with endoplasmic reticulum-derived vesicles during virus infection. *Plant Physiol.* **138**:1877–1895.
- Jurgens, G. 2004. Membrane trafficking in plants. *Annu. Rev. Cell Dev. Biol.* **20**:481–504.
- Kawakami, S., Y. Watanabe, and R. N. Beachy. 2004. *Tobacco mosaic virus* infection spreads cell to cell as intact replication complexes. *Proc. Natl. Acad. Sci. USA* **101**:6291–6296.
- Kikumoto, T., and C. Matsui. 1961. Electron microscopy of intracellular *Potato virus X*. *Virology* **13**:294–299.
- Kozar, F. E., and Y. M. Sheludko. 1969. Ultrastructure of potato and *Datura stramonium* plant cells infected with *Potato virus X*. *Virology* **38**:220–229.
- Krishnamurthy, K., M. Heppler, R. Mitra, E. Blancaflor, M. Payton, R. S. Nelson, and J. Verchot-Lubicz. 2003. The *Potato virus X* TGBp3 protein associates with the ER network for virus cell-to-cell movement. *Virology* **309**:135–151.
- Krishnamurthy, K., R. Mitra, M. E. Payton, and J. Verchot-Lubicz. 2002. Cell-to-cell movement of the PVX 12K, 8K, or coat proteins may depend on the host, leaf developmental stage, and the PVX 25K protein. *Virology* **300**:269–281.
- Liu, J. Z., E. B. Blancaflor, and R. S. Nelson. 2005. The *Tobacco mosaic virus* 126-kilodalton protein, a constituent of the virus replication complex, alone or within the complex aligns with and traffics along microfilaments. *Plant Physiol.* **138**:1853–1865.
- Liu, Y., M. Schiff, K. Czymmek, Z. Tallozy, B. Levine, and S. P. Dinesh-Kumar. 2005. Autophagy regulates programmed cell death during the plant innate immune response. *Cell* **121**:567–577.
- Lough, T. J., N. E. Netzler, S. J. Emerson, P. Sutherland, F. Carr, D. L. Beck, W. J. Lucas, and R. L. Forster. 2000. Cell-to-cell movement of potexviruses: evidence for a ribonucleoprotein complex involving the coat protein and first triple gene block protein. *Mol. Plant-Microbe Interact.* **13**:962–974.
- Lough, T. J., K. Shash, B. Xoconostle-Cázares, K. R. Hofstra, D. L. Beck, E. Balmori, R. L. S. Forster, and W. J. Lucas. 1998. Molecular dissection of the mechanism by which potexvirus triple gene block proteins mediate cell-to-cell transport of infectious RNA. *Mol. Plant Microbe Interact.* **11**:801–814.
- Lucas, W. J. 2006. Plant viral movement proteins: agents for cell-to-cell trafficking of viral genomes. *Virology* **344**:169–184.
- Martelli, G. P., and W. Jelkmann. 1998. *Foveavirus*, a new plant virus genus. *Arch. Virol.* **143**:1245–1249.
- Memelink, J., C. I. van der Vlugt, H. J. Linthorst, A. F. Derks, C. J. Asjes, and J. F. Bol. 1990. Homologies between the genomes of a carlavirus (*Lily*

- symptomless virus*) and a potexvirus (*Lily virus X*) from lily plants. J. Gen. Virol. **71**:917–924.
37. Meshi, T., D. Hosokawa, M. Kawagishi, Y. Watanabe, and Y. Okada. 1992. Reinvestigation of intracellular localization of the 30K protein in tobacco protoplasts infected with *Tobacco mosaic virus* RNA. Virology **187**:809–813.
 38. Mitra, R., K. Krishnamurthy, E. Blancaflor, M. Payton, R. S. Nelson, and J. Verchof-Lubicz. 2003. The *Potato virus X* TGBp2 protein association with the endoplasmic reticulum plays a role in but is not sufficient for viral cell-to-cell movement. Virology **312**:35–48.
 39. Nagata, T., Y. Nemoto, and S. Hasezawa. 1992. Tobacco BY-2 cell line as the “Hela” cell in the cell biology of higher plants. Int. Rev. Cytol. **132**:1–31.
 40. Nebenfuhr, A. 2002. Vesicle traffic in the endomembrane system: a tale of COPs, RabS and SNAREs. Curr. Opin. Plant Biol. **5**:507–512.
 41. Palacios, S., L. H. Perez, S. Welsch, S. Schleich, K. Chmielarska, F. Melchior, and J. K. Locker. 2005. Quantitative SUMO-1 modification of a vaccinia virus protein is required for its specific localization and prevents its self-association. Mol. Biol. Cell **16**:2822–2835.
 42. Peremyslov, V. V., Y. W. Pan, and V. V. Dolja. 2004. Movement protein of a closterovirus is a type III integral transmembrane protein localized to the endoplasmic reticulum. J. Virol. **78**:3704–3709.
 43. Qi, Y., and B. Ding. 2002. Replication of *Potato spindle tuber viroid* in cultured cells of tobacco and *Nicotiana benthamiana*: the role of specific nucleotides in determining replication levels for host adaptation. Virology **302**:445–456.
 44. Randles, J. W., and W. Rohde. 1990. *Nicotiana velutina* mosaic virus: evidence for a bipartite genome comprising 3 kb and 8 kb RNAs. J. Gen. Virol. **71**:1019–1027.
 45. Restrepo-Hartwig, M., and P. Ahlquist. 1999. *Brome mosaic virus* RNA replication proteins 1a and 2a colocalize and 1a independently localizes on the yeast endoplasmic reticulum. J. Virol. **73**:10303–10309.
 46. Rouleau, M., R. J. Smith, J. B. Bancroft, and G. A. Mackie. 1994. Purification, properties, and subcellular localization of foxtail mosaic potexvirus 26-kDa protein. Virology **204**:254–265.
 47. Salonen, A., T. Ahola, and L. Kaariainen. 2005. Viral RNA replication in association with cellular membranes. Curr. Top. Microbiol. Immunol. **285**: 139–173.
 48. Schaad, M. C., P. E. Jensen, and J. C. Carrington. 1997. Formation of plant RNA virus replication complexes on membranes: role of an endoplasmic reticulum-targeted viral protein. EMBO J. **16**:4049–4059.
 49. Schepetilnikov, M. V., U. Manske, A. G. Solovyev, A. A. Zamyatnin, Jr., J. Schiemann, and S. Y. Morozov. 2005. The hydrophobic segment of *Potato virus X* TGBp3 is a major determinant of the protein intracellular trafficking. J. Gen. Virol. **86**:2379–2391.
 50. Schwartz, M., J. Chen, M. Janda, M. Sullivan, J. den Boon, and P. Ahlquist. 2002. A positive-strand RNA virus replication complex parallels form and function of retrovirus capsids. Mol. Cell **9**:505–514.
 51. Schwartz, M., J. Chen, W. M. Lee, M. Janda, and P. Ahlquist. 2004. Alter-
nate, virus-induced membrane rearrangements support positive-strand RNA virus genome replication. Proc. Natl. Acad. Sci. USA **101**:11263–11268.
 52. Siemering, K., R. M. Golbik, R. Sever, and J. Haseloff. 1996. Mutations that suppress the thermosensitivity of green fluorescent protein. Curr. Biol. **6**:1653–1663.
 53. Solovyev, A. G., T. A. Stroganova, A. A. Zamyatnin, Jr., O. N. Fedorkin, J. Schiemann, and S. Y. Morozov. 2000. Subcellular sorting of small membrane-associated triple gene block proteins: TGBp3-assisted targeting of TGBp2. Virology **269**:113–127.
 54. Suhy, D. A., T. H. Giddings, Jr., and K. Kirkegaard. 2000. Remodeling the endoplasmic reticulum by *Poliovirus* infection and by individual viral proteins: an autophagy-like origin for virus-induced vesicles. J. Virol. **74**:8953–8965.
 55. Turina, M., B. Desvoyes, and K. B. Scholthof. 2000. A gene cluster encoded by *Panicum mosaic virus* is associated with virus movement. Virology **266**: 120–128.
 56. Turner, R. L., P. R. Mills, and G. D. Foster. 1993. Nucleotide sequence of the 7 K gene of *Helenium virus* S. Acta Virol. **37**:523–528.
 57. Vilar, M., A. Sauri, M. Monne, J. F. Marcos, G. von Heijne, E. Perez-Paya, and I. Mingarro. 2002. Insertion and topology of a plant viral movement protein in the endoplasmic reticulum membrane. J. Biol. Chem. **277**:23447–23452.
 58. Voinnet, O., C. Lederer, and D. C. Baulcombe. 2000. A viral movement protein prevents spread of the gene silencing signal in *Nicotiana benthamiana*. Cell **103**:157–167.
 59. Yang, Y., B. Ding, D. C. Baulcombe, and J. Verchof. 2000. Cell-to-cell movement of the 25K protein of *Potato virus X* is regulated by three other viral proteins. Mol. Plant-Microbe Interact. **13**:599–605.
 60. Yang, Y. D., R. Elamawi, J. Bubeck, R. Pepperkok, C. Ritzenthaler, and D. G. Robinson. 2005. Dynamics of COPII vesicles and the Golgi apparatus in cultured *Nicotiana tabacum* BY-2 cells provides evidence for transient association of Golgi stacks with endoplasmic reticulum exit sites. Plant Cell **17**:1513–1531.
 61. Zamyatnin, A. A., Jr., A. G. Solovyev, P. V. Bozhkov, J. P. Valkonen, S. Y. Morozov, and E. I. Savenkov. 2006. Assessment of the integral membrane protein topology in living cells. Plant J. **46**:145–154.
 62. Zamyatnin, A. A., Jr., A. G. Solovyev, A. A. Sablina, A. A. Agranovsky, L. Katul, H. J. Vetten, J. Schiemann, A. E. Hinkkanen, K. Lehto, and S. Y. Morozov. 2002. Dual-colour imaging of membrane protein targeting directed by *Poa semilatent virus* movement protein TGBp3 in plant and mammalian cells. J. Gen. Virol. **83**:651–662.
 63. Zamyatnin, A. A., Jr., A. G. Solovyev, E. I. Savenkov, A. Germundsson, M. Sandgren, J. P. Valkonen, and S. Y. Morozov. 2004. Transient coexpression of individual genes encoded by the triple gene block of *Potato mop-top virus* reveals requirements for TGBp1 trafficking. Mol. Plant-Microbe Interact. **17**:921–930.